Applied Physics B (2023) 129:31
https://doi.org/10.1007/s00340-023-07971-7

Applied Physics B
Lasers and Optics

RESEARCH

Experimental and theoretical investigations on the modulation capabilities of a sample of vertical cavity surface emitting laser diodes for atomic vapour applications

Christoph Amtmann[1] · Roland Lammegger[1] · Alexander Betzler[1] · Martín Agú[2] · Michaela Ellmeier[2] · Christian Hagen[2] · Irmgard Jernej[2] · Werner Magnes[2] · Andreas Pollinger[2] · Wolfgang E. Ernst[1]

Received: 29 September 2022 / Accepted: 9 January 2023 / Published online: 27 January 2023

Abstract
This paper discusses various frequency modulation and intensity modulation capabilities within a sample of direct laser current modulated identical vertical cavity surface emitting laser diodes. The presented analysis is based on measurements of the spectral amplitudes as a function of the applied modulation power at a constant modulation frequency of 3.517 GHz. Their evaluation by Bessel function fits produces the three modulation parameters: frequency modulation index, intensity modulation index (via the α parameter) and the side band asymmetry of the first order side bands. The variation of the laser diode's modulation capability is discussed. It is found that the individual laser diodes show a significant variations in their modulation capabilities. Thus an experimental preselection of the laser diode is required to find laser diodes which are suitable as a light source for atomic vapour applications, with special emphasis on a coherent population trapping-based scalar magnetometers.

Keywords Vertical cavity surface emitting laser · VCSEL · Direct laser current modulation · Frequency modulation · Intensity modulation · Atomic vapour

✉ Christoph Amtmann
christoph.amtmann@tugraz.at

Roland Lammegger
roland.lammegger@tugraz.at

Alexander Betzler
alexander.betzler@tugraz.at

Martín Agú
martin.agu@oeaw.ac.at

Michaela Ellmeier
michaela.ellmeier@tugraz.at

Irmgard Jernej
irmgard.jernej@oeaw.ac.at

Werner Magnes
werner.magnes@oeaw.ac.at

Andreas Pollinger
andreas.pollinger@oeaw.ac.at

Wolfgang E. Ernst
wolfgang.ernst@tugraz.at

[1] Institute of Experimental Physics, Graz University of Technology, Petersgasse 16, Graz 8010, Austria

[2] Space Research Institute, Austrian Academy of Sciences, Schmiedlstraße 6, Graz 8042, Austria

1 Introduction

In many atomic vapour applications, such as optical magnetometers and atomic clocks, vertical cavity surface emitting lasers (VCSEL) are used as light source due to their low power consumption, ease of use and direct current modulation capabilities with modulation frequencies in the GHz regime [1].

For this work, the application of interest is the Coupled Dark State Magnetometer (CDSM) [2], which is a coherent population trapping (CPT) [3] based scalar and omni-directional magnetometer, especially designed for scientific space missions [4, 5]. It couples two magnetically dependent CPT resonances within the hyperfine manifold of the ^{87}Rb D_1 line. A VCSEL diode was selected as coherent light source. It emits at a wavelength of about 795 nm and is frequency modulated (FM) with approx. 3.417 GHz to create two first order side bands to match the hyperfine ground state splitting of approx. 6.834 GHz. This frequency modulation is achieved with a modulation of the laser bias current [6] which also produces a residual intensity modulation (IM) of the emitted laser light [7].

This IM influences the first order side band amplitudes and therefore the excitation of the CPT resonances used for CDSM's measurement principle.

In 2018, the CDSM was launched into space the first time on-board the China Seismo-Electromagnetic Satellite (CSES) [8]. The upcoming JUpiter ICy moons Explorer (JUICE) mission of the European Space Agency will be one of its next space applications. JUICE aims to explore the Jupiter system and its Galilean moons Ganymede, Callisto and Europa in terms of their potentially habitable environments [9]. The launch is scheduled for mid-2023 with an expected arrival at the Jupiter system in 2031. The scalar CDSM is part of the three-sensor magnetometer J-MAG which also includes two fluxgate sensors measuring also the direction of the magnetic field. For both missions, the CDSM acts as reference for an improval of the overall accuracy of the magnetic field measurement.

For this mission, a suitable 795 nm single mode VCSEL diode in a tilted TO-46 cap (*APM2101013300*) had to be selected from a laser diode sample from the manufacturer *II-VI Laser Enterprise*. The CDSM's functional principle as well as its application in space dictate the VCSEL selection criteria. The long term stability and endurance of the laser diodes under vacuum conditions were investigated in [10]. Although the laser diodes are specified as single mode emitter, a preselection in terms of additional laser frequency modes resulted in a total number of 10 out of 18 suitable laser diodes.

The correct instrument operation requires the first order side bands to have equal amplitudes to allow a balanced excitation of the CPT resonances. Deviations from this ratio can cause light shift effects [11–13] and resonance shape deformations [14] which in turn influence the CDSM's accuracy. For an efficient CPT excitation, the spectral amplitudes of the first order side bands should be maximised. For a pure frequency modulation of the laser light, described by Bessel functions of the first kind, the maximum first order side band amplitudes are reached at the frequency modulation index $m_F = 1.84$.

During the JUICE mission, the optical fibres and optical components used within the sensor unit are exposed to high energy particle radiation over the long period of 17 years. This leads to a constantly increasing damping of the transmitted optical power. To counteract this, the laser diode is tuned to a higher optical output power by increasing the laser bias current. Therefore, the first order side band amplitude requirements have to be fulfilled for a large range of laser bias current.

This paper will show the variations of the modulation capabilities within the sample of VCSEL diodes. This is achieved by an experimental investigation of the laser spectra as a function of applied microwave power as well as a mathematical analysis based on fits with Bessel functions of the first kind. From an application based standpoint, the diode's interchangeability is discussed.

2 Theoretical description

The behaviour of a semiconductor laser is described in terms of the reservoir model with carrier and photon density rate equations [15, p. 248]. The variation in the laser bias current results in the change of the laser output power and thus in a laser light intensity modulation. The laser bias current is the driving force of the system's perturbation. The response to such a perturbation is described in the context of the dynamic small signal frequency response [15]. Differential rate equations are used for its description [15, p. 259].

The IM response to a sinusoidal modulation with modulation frequency ω_m is described by the modulation transfer function [7]

$$H(\omega) = \frac{\omega_R^2}{\omega_R^2 - \omega_m^2 + i\omega_m\gamma}, \tag{1}$$

with ω_R the relaxation resonance frequency and γ the system's damping factor. γ describes the intrinsic modulation bandwidth capabilities of the laser [15, p. 265] and is [15, p. 262]

$$\gamma = \gamma_{PP} + \gamma_{NN}. \tag{2}$$

γ_{PP} is related to the effective photon lifetime [7, 15] and γ_{NN} to the differential carrier lifetime. The larger the lifetimes, the less the system is susceptible to current changes at high frequencies, which results in an increase of high frequency damping. The modulation transfer function acts like a second-order low-pass filter with a damped resonance close to the cutoff frequency [15, p. 262].

Figure 1 shows the absolute value of the IM response function. Near its resonance, the amount of intensity modulation is the largest and drops off significantly for higher modulation frequencies.

Above the threshold current I_{th}, the relaxation resonance frequency is a function of the laser bias current I [15, p. 265] [15, p. 73]

$$\omega_R \propto \left[I - I_{th}\right]^{1/2}. \tag{3}$$

This shows, that an intensity modulation at higher bias currents results in a resonance peak at higher modulation frequencies. This is experimentally presented, e.g., in [1] and [15, p. 266].

The IM response is proportional to the modulation transfer function $H(\omega_m)$, which relates the output of a system to its input. This allows to write [7]

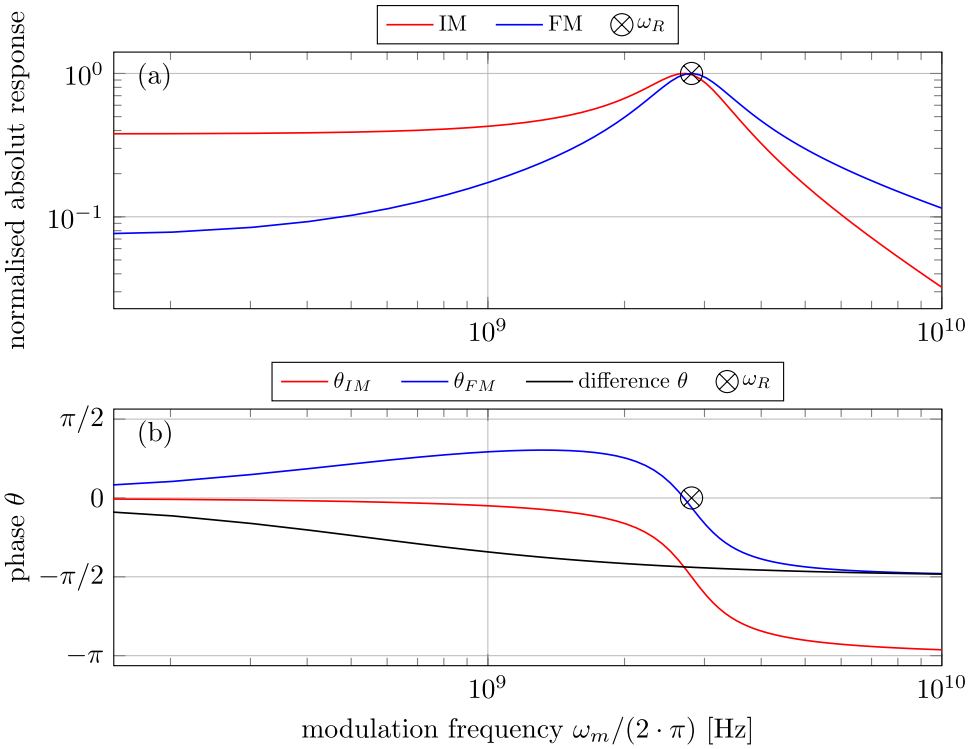

Fig. 1 **a** Normalised response functions for the FM and IM behaviour according to Eqs. 1 and 5. **b** Phases θ_{IM} and θ_{FM} of the response functions and their difference. For the calculation, the values $\gamma = 6.8\times10^9, s^{-1}\gamma_{PP} = 3.4\times10^9, s^{-1}$ and $\omega_R/2\pi = 2.81\times10^{10}$ Hz were taken from [7]

$$\frac{P_m}{I_m} \propto H(\omega_m), \tag{4}$$

with P_m the modulation output power at the frequency ω_m and I_m the modulation current.

A laser current modulation of the laser's active region results in a modulation of the charge carrier and photon density. This charge carrier density modulation effects the gain and the index of refraction of the active region. Therefore, the cavity optical length is modulated by the current and causes its resonant mode to shift in frequency [15, p. 270]. This determines the laser output frequency and the IM and FM modulations are intrinsically linked for direct laser current modulation.

The FM response of the system is [7][15, p. 271]

$$\frac{\nu_1}{I_m} \propto \left(\gamma_{PP} + i\omega_m\right)H(\omega_m). \tag{5}$$

With ν_1 the modulated optical frequency and the modulation current I_m.

In figure 1 (a) the normalised absolute value of the complex IM and FM response functions are shown. In (b), their phase relations θ_{IM} and θ_{FM}, calculated by the argument of the complex function (equations 1 and 5) as well as the phase difference $\theta = \theta_{IM} - \theta_{FM}$ are displayed. Both modulations show a resonance peak, however the peaks do not coincide. The used scaling of figure 5(a) does not resolve the separation of the peaks for the selected calculation parameters. The IM resonance peak appears at lower modulation frequencies compared to the FM modulation [15, p. 272]. The IM modulation is more efficient at modulation frequencies $\omega_m \ll \omega_R$, the FM modulation is more efficient at $\omega_m \gg \omega_R$.

The ratio of the FM index m_F to the IM index m_I is defined as [15, p. 272]

$$\frac{m_F}{m_I} = \frac{\alpha}{2}\sqrt{\left(\frac{\gamma_{PP}}{\omega_m}\right)^2 + 1}. \tag{6}$$

For large modulation frequencies $\omega_m \gg \gamma_{PP}$ this equation becomes

$$\frac{m_F}{m_I} = \frac{\alpha}{2}. \tag{7}$$

In Fig. 1(b) for large modulation frequencies and $\gamma_{PP} = 3.4\times10^9$ rad s^{-1}, the difference between the IM and FM phase becomes $-\pi/2$ while for lower modulation frequencies the phase difference approaches 0. Typical values for α are between 4 and 6 [15, p. 271].

2.1 Frequency modulation with residual intensity modulation

In [16], a general modulated electric component of the laser light field is

$$E(t) = M(t)\cdot e^{i\omega t}, \tag{8}$$

with $M(t)$ the complex modulation function and ω the optical frequency. Direct laser current modulation with a sinusoidal laser current at the modulation frequency ω_m results in the amplitude modulated laser current $I(t) = I_0 + I_m \cdot \sin(\omega_m t)$, where I_0 is the laser bias current and I_m the modulation current. By assuming a linear laser current to output power characteristic and $I(t)$ above the laser threshold, the laser optical output power becomes $P(t) = P_0 + P_m \cdot \sin(\omega_m t)$, where P_0 is the unmodulated and P_m the modulation output power.

With the normalisation $P(t)/P_0$, the normalised output power is [16]

$$p(t) = 1 + \frac{P_m}{P_0} \cdot \sin(\omega_m t) = 1 + m_I \cdot \sin(\omega_m t). \tag{9}$$

The intensity modulation index is given as

$$m_I = \frac{P_m}{P_0}. \tag{10}$$

The output power is proportional to the square of the electric field $P(t) \propto |E|^2 \propto |M(t)|^2$, thus the normalised modulation function becomes [16]

$$|m_{IM}(t)| = \sqrt{1 + m_I \cdot \sin(\omega_m t)}. \tag{11}$$

As described in the previous section, direct laser current modulation creates frequency modulation at the modulation frequency ω_m. To include this, the entire normalised (frequency and intensity) modulated signal $m(t)$ is [16]

$$m(t) = \sqrt{1 + m_I \sin(\omega_m t + \theta_{IM})} \cdot e^{i \cdot m_F \cdot \cos(\omega_m t + \theta_{FM})}. \tag{12}$$

m_F is the frequency modulation index and θ_{IM} and θ_{FM} are the IM and FM phases. Their phase difference is $\theta = \theta_{IM} - \theta_{FM}$.

For the IM index $m_I < 1$ Eq. 11 is approximated as a Taylor series with [16]

$$m_{IM}(t) \simeq 1 + \frac{m_I}{2} \cdot \sin(\omega_m t). \tag{13}$$

The resulting laser power spectrum P (with the approximation from Eq. 13) can be expressed as the sum of Bessel functions of the first kind [16]

$$\begin{aligned} P(\omega_m) = \sum_{n=-\infty}^{\infty} & |J_n(m_F) - \frac{m_I}{4}\big(J_{n+1}(m_F) \cdot e^{i\theta} \\ & + J_{n-1}(m_F) \cdot e^{-i\theta}\big)|^2 \\ & \cdot \delta(\omega - n \cdot \omega_m). \end{aligned} \tag{14}$$

From this, the normalised n^{th} order side band amplitude (optical power within spectral component) is

$$a_n = |J_n(m_F) - \frac{m_I}{4}\big(J_{n+1}(m_F) \cdot e^{i\theta} + J_{n-1}(m_F) \cdot e^{-i\theta}\big)|^2. \tag{15}$$

The side bands with the same order have an equal amplitude $a_{\pm n}$ for the entire m_F range, if $m_I = 0$ or the phase difference θ is an odd multiple of $\pi/2$ [7]. The evaluation for constant modulation indices ($m_I \neq 0$) of Eq. 15 shows, that for $\pi > \theta > |\pi/2|$, the first order a_{+n} side band amplitude is larger than the a_{-n} amplitude, while for $0 < \theta < |\pi/2|$, the a_{-n} amplitude is larger than the a_{+n}.

A frequency modulation index of $m_F = 1.84$ and an intensity modulation index of $m_I = 0$ result in the maximum amplitude of both first order side band [1]. The carrier amplitude a_0 becomes 0 at $m_F = 2.41$ while $m_I = 0$ or for $m_I \neq 0$ when $\theta = 0$.

Since a high first order side band symmetry is desired for equal atomic excitation, an asymmetry factor A_1 is defined [17, p. 37]

$$A_1 = 10 \cdot \log\left(\frac{a_{-1}}{a_{+1}}\right), \tag{16}$$

with a_{-1} the lower and a_{+1} the upper first order side band amplitude of the modulated laser light.

3 Measurement setup

For space missions, a compact instrument is built which includes an electronics box, a sensor unit and optical fibres. The CDSM's sensor unit is built around a spectroscopic glass cell filled with ^{87}Rb and neon as buffer gas [5, 18]. Optical fibres guide the laser light from the laser diode to the sensor unit and back to the photodiode. The sensor is mounted on a boom, several meters away, to minimise magnetic disturbances introduced by the satellite.

A representative hardware of the flight model for the JUICE mission was used to evaluate the laser diodes' modulation capabilities. The hardware creates and controls the microwave frequency, the modulation (microwave) power P_{mw}, the laser bias current as well as the laser temperature for the here discussed experiments. The microwave power P_{mw} started from −25.8 dBm and was increased to 1.3 dBm with 0.5 dB steps. A schematic diagram of the hardware's functional blocks is shown in Fig. 2.

In the electronics box, the VCSEL diode is installed within a custom diode housing. This housing is equipped with a Pt1000 platinum resistor and a Peltier element for the laser diode temperature control. For a given laser bias current, the laser temperature was varied to tune the laser's output frequency close to the ^{87}Rb D_1 line. A RG-402 cable guides the microwave signal from the microwave generator to the laser diode. The change in the microwave power influences the modulation behaviour of the diode and therefore the emitted light spectrum. The laser spectra were analysed with the scanning Fabry-Perot Interferometer (FPI)

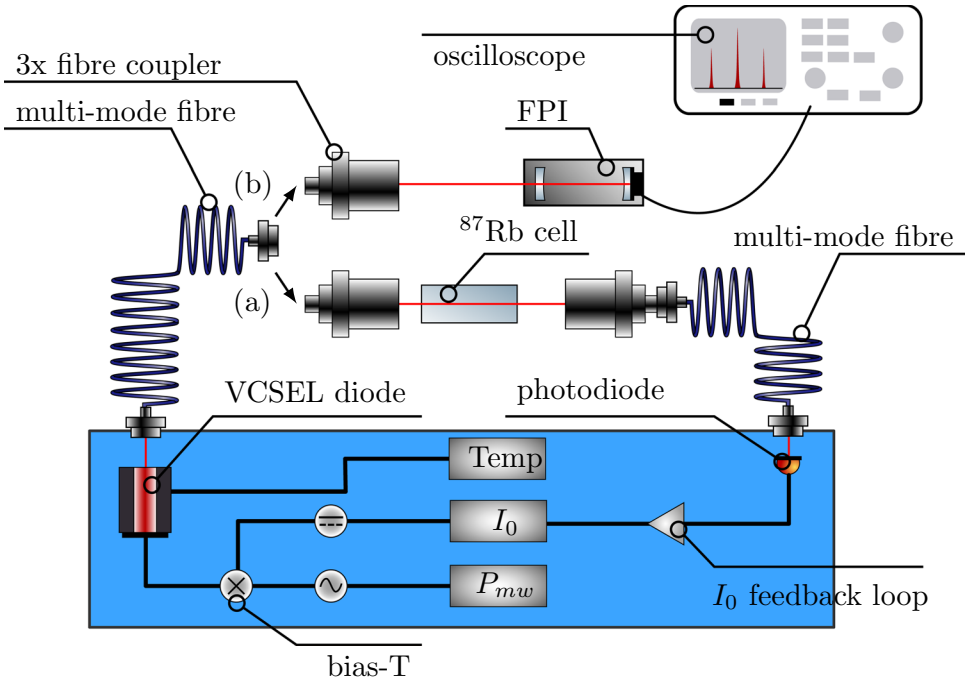

Fig. 2 Experimental setup (**a**) locks the laser bias current I_0 feedback loop to the ^{87}Rb D_1 line for the stabilisation of the laser output frequency. Experimental setup (**b**) detects the amplitudes of the light's spectral components with the Fabry-Perot interferometer (FPI). The blue box represents the CDSM hardware

SA210-5B from *ThorLabs*. This device has a free spectral range of 10 GHz and a resolution of 67 MHz (> 150 finesse).

The 10 GHz free spectral range of the FPI results in an unfavorable overlap of the first and second order side bands for the modulation frequency of 3.417 GHz when observed on the oscilloscope. To separate these spectral components on the oscilloscope, the modulation frequency was changed to 3.517 GHz.

For the laser diode housing, including one of the laser diodes under test, the coefficient of input reflection S_{11}[19, p. 1178] was measured with the *R54 GHz Analyzer* from *Copper Mountain Technologies*. This allows to quantify the effective microwave power received by the laser diode chip. In Fig. 3 the S_{11} coefficient as a function of the applied laser bias current is shown. For both tested microwave powers and investigated microwave frequencies, the input reflection coefficient shows a linearly decreasing behaviour.

4 Exemplary spectra of a VCSEL laser diode

In Fig. 4 the measured modulation spectrum for an exemplary laser diode from the investigated sample is displayed. Four different laser bias currents were applied and the laser light's spectral amplitudes were recorded as a function of the modulation (microwave) power P_{mw}. The spectral

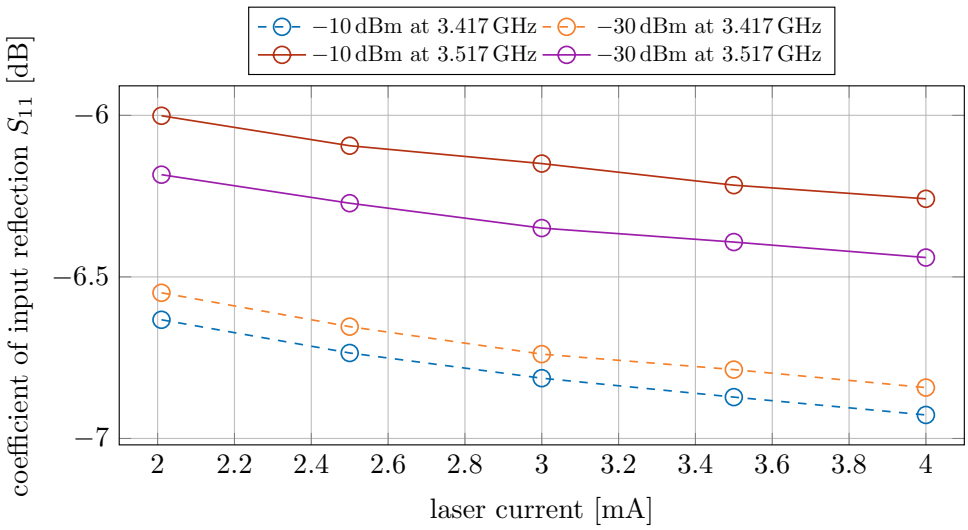

Fig. 3 Coefficient of input reflection S_{11} for the custom laser diode housing with a representative VCSEL diode as a function of the applied laser bias current. Two different microwave powers at two different modulation frequencies were investigated

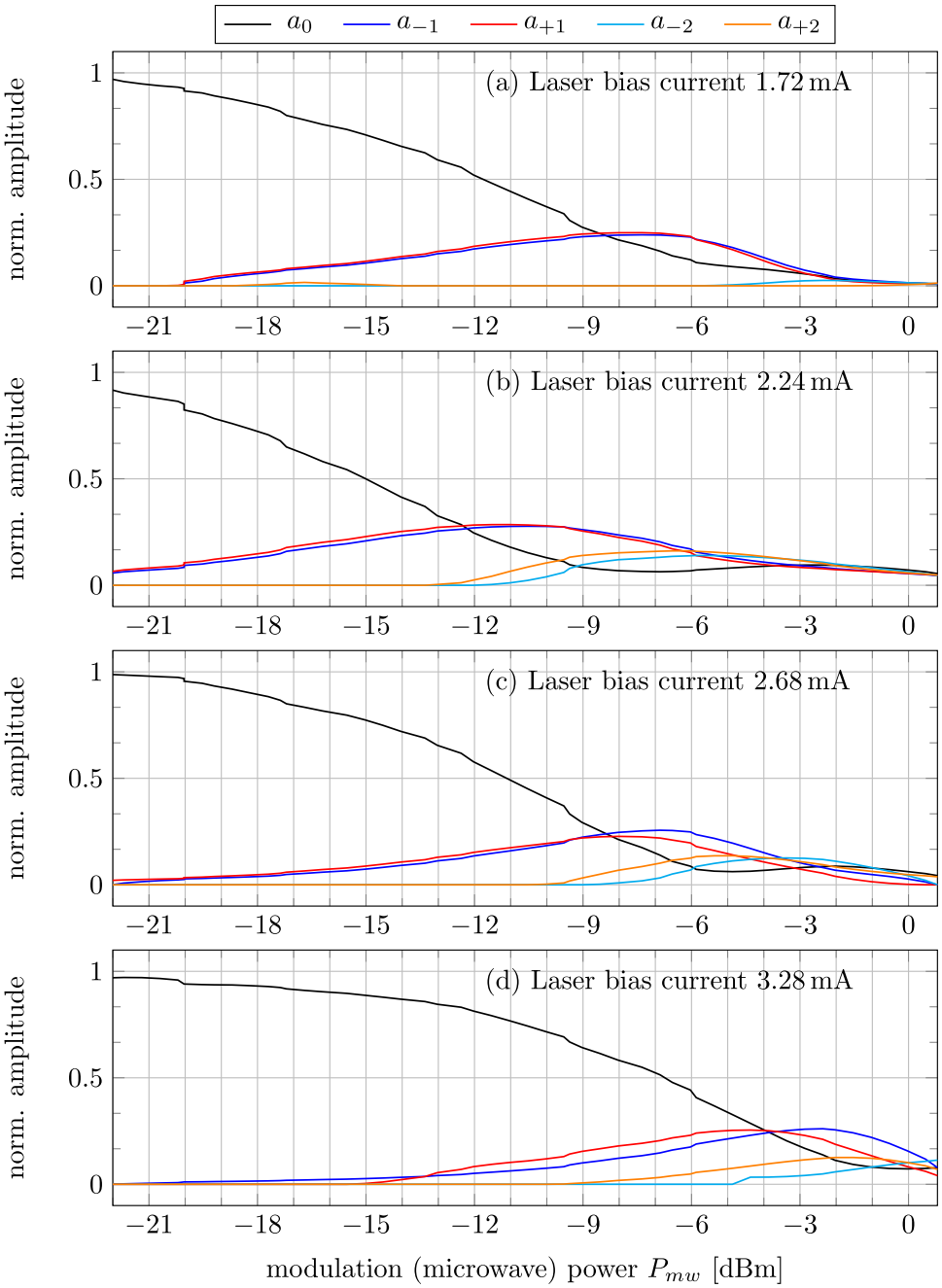

Fig. 4 Exemplary laser diode spectrum as a function of the applied modulation power P_{mw}, measured at four different laser bias currents with a Fabry-Perot interferometer. The modulation frequency was constant at 3.517 GHz. The normalised n^{th} order side band amplitude are labelled as a_n

amplitudes are normalised with the carrier amplitude measured at $P_{mw} = -25.8$ dBm. At this modulation power only the carrier amplitude is detectable with the FPI. The depicted (Fig. 4) and analysed P_{mw} range starts at −22.0 dBm and goes to 0.8 dBm.

The modulation frequency was $\omega_m = 2\pi \cdot 3.517$ GHz. For each laser bias current, the laser temperature was set such that the diode emits light close to the ^{87}Rb D_1 line and was kept constant while the microwave power was increased. Equation 3 shows that ω_R increases for larger laser bias currents, which shifts the maxima shown in Fig. 1a to higher frequencies. The modulation frequency ω_m is kept constant for all experiments. This means, that the frequency difference between ω_m and ω_R is changed as a function of the laser bias current. The interplay between these two frequencies determines the laser diode's modulation behaviour. ω_R was not directly measured in the context of this work.

Due to the diode's (partial) AC rectification, the increasing microwave power adds an additional DC to the constant (supply) bias current. With higher effective bias current, the relaxation resonance frequency ω_R is shifted to higher frequencies. This reduces the FM-IM phase difference θ at the

constant modulation frequency ω_m (see Fig. 1b). Thus the changes in θ, due to higher P_{mw}, are increased. The slope $\partial\theta/\partial P_{mw}$ changes as a function of the laser bias current.

For the laser current of 1.72 mA in Fig. 4a, the first order side bands amplitudes are nearly equal over a wide modulation power range. The IM is weak which indicates that ω_m is larger than ω_R and therefore, the phase difference between both modulations is close to $\theta = -\pi/2$ as shown by the simple model of Fig. 1b, this explains the high symmetry of the side band amplitudes.

The spectral amplitudes measured at the laser bias current of 2.24 mA are shown in Fig 4b. The first order side band amplitude maxima are found at a lower microwave power of about −10.5 dBm compared to the measurements at 1.72 mA, therefore the modulation is more efficient. This indicates, that the increased laser bias current pushes the response maximum (at about ω_R) closer to ω_m. For the first and second order side bands a change in the amplitude trend is visible. For lower microwave powers, the upper side band amplitudes are larger while for a higher microwave powers the lower side bands become larger.

For laser bias currents $I > 2.24$ mA, the first order side bands maxima appear at higher modulation powers. The amplitude difference in the side bands becomes more pronounced which results in a reduction of the microwave power ranges with equal side band amplitudes. Additionally, the side band maxima of the same order are separated and are not observed at the same modulation powers. Furthermore, the ranges of equal amplitudes for the first and second order side bands are not found at the same modulation powers.

For the laser bias current of 2.68 mA (Fig. 4c), the first order maximum amplitudes appear at higher modulation powers, which indicates, that the modulation efficiency is smaller than in (b). For the higher laser bias current, ω_R is further pushed to higher frequencies. The reduction in modulation efficiency suggests that ω_m is now lower than ω_R which can be explained with Fig. 1a. For $\omega_m < \omega_R$, the FM response drops faster than the IM response, thus the IM becomes more pronounced which explains the measured increase in first and second order side band asymmetry.

An increase in modulation power results in an additional DC laser bias current which shifts the relaxation response frequency ω_R to higher values. For $\omega_m < \omega_R$ a higher effective bias current shifts the phase difference θ closer to 0, see Fig. 1b. This is not particularly prominent for $\omega_m > \omega_R$, due to the nearly constant $\partial\theta/\partial P_m$ slope.

In Fig. 4c, a significant change in the amplitude trend is visible. Until about −10.5 dBm, the a_{+1} amplitude is larger than a_{-1} and for higher powers, the a_{-1} amplitude is dominant. This can be explained with the mentioned modulation power introduced θ shift. For low modulation powers $\theta < -\pi/2$, which results in larger a_{+n} amplitudes, for $\theta = -\pi/2$, the amplitudes are equal, and for $\theta > -\pi/2$, the a_{-n} are larger. For the second order side bands, the upper amplitude is larger until the trend changes at about – 4 dBm.

Figure 4c shows, that each side band order has the modulation power for equal amplitudes at different modulation powers, which can be explained by Eq. 15 when θ is assumed to be different for each side band order. This is a contradiction to the presented simple dynamic small signal model which includes only one θ for all spectral components (Eq. 14). From Fig. 1b, it is expected that $\theta = -\pi/2$ can not be surpassed, but the measurements indicate that $\theta > |\pi/2|$ at higher laser bias currents with low modulation powers.

At the bias current of 3.28 mA in Fig. 4d, the first order side band amplitudes for low microwave powers are not equal. The effects observed for the laser bias current in Fig. 4c are more pronounced. The first and second order side band maxima are further separated and pushed to higher modulation powers. The modulation powers for symmetric first order side band amplitudes are limited to a very narrow range.

In general, an increase in laser bias current results in a stronger IM modulation. The laser diode's data sheet lists the maximum laser bias current as 4 mA. However, Fig. 4 shows that already at a bias current of 3.28 mA only a narrow range of microwave powers leads to symmetric first order side band amplitudes. This limits the bias current range suitable for direct laser current modulation. High optical output powers, caused by high laser bias currents are not accessible under the consideration of symmetric first order side band amplitudes.

The diode's modulation efficiency is defined by the diode's intrinsic behaviour not by the measurement setup, since the setup's reflection measurement (Fig. 3), shows a linear behaviour and the modulation efficiency peaks at about 2.24 mA.

The presented modulation behaviour is typical for the entire sample of laser diodes. However, the modulation efficiencies and the amplitude asymmetries at a given modulation power and the maximum usable bias currents differ significantly between the diodes. Therefore, the results for the entire sample are presented to show the general modulation capabilities and the variations of specific parameters.

5 Fit approach of spectral components

For each laser diode of the sample, the spectral amplitudes were measured at several laser bias currents as a function of the applied modulation power, as shown for an exemplary VCSEL diode in Fig. 4. For each laser bias current, the measured data set was fitted simultaneously for all measured spectral components (carrier, first and second order side band amplitudes) at all modulation powers P_{mw} with a combined set of individual fit functions with shared fit

parameters. Therefore, Eq. 15 is evaluated for each spectral component for the fit parameters $m_F(P_{mw})$, $\theta(P_{mw})$ and m_I.

The best fitting results were achieved with the following additional assumptions:

- For the determination of the m_F a linear relation between the applied microwave power P_{mw} and m_F was assumed. This idea is based on the results presented in [20] which show a linear relation between m_F and P_{mw}. With this, a frequency modulation index can be associated for each measured modulation power.
- For low bias current, θ was assumed to be constant for all spectral components, due to the flat slope $\partial\theta/\partial P_{mw}$ as show in Fig. 1b for $\omega_m > \omega_R$.
- For larger laser bias current, θ was assumed to change with the microwave power due to an increased $\partial\theta/\partial P_{mw}$ slope (Fig. 1b).
- For larger bias currents, each pair of side bands was associated with its own phase θ as it was indicated by the measurements of Fig. 4c and d. The threshold current which separated the lower and larger laser bias currents depends on the modulation capabilities of each laser diode and had to be adjusted individually.
- The intensity modulation index m_I is linked to m_F with Eq. 7. Therefore, α was used as a fit parameter.

The fits were performed with Matlab and the *lsqcurvefit* function. This non-linear least square routine allows to fit all spectral components with individual fit functions but with shared fit parameters simultaneously.

6 Discussion of the measured modulation capabilities

The following analysis includes FPI measurements of the spectral amplitudes at several laser bias currents and constant modulation frequency of 3.517 GHz for the 10 investigated laser diodes. Figure 5 shows the required microwave powers P_{mw} to achieve the frequency modulation indices m_F of 1.50, 1.84 and 2.41 as a function of the laser bias current. For the entire sample, the most efficient modulation occurs at the laser bias current range around 2.1 mA. This is also reflected by the investigation of the exemplary laser diode in Sect. 4.

The $\alpha = \frac{2 \cdot m_F}{m_I}$ parameter as a function of the laser bias current is shown in Fig. 6 for all laser diodes. The highest values for α correspond to the lowest intensity modulation index m_I. Starting at about 2.2 mA, the α parameters start to spread more compared to the lower currents. This means the intensity modulation variations within the sample are more prominent for larger laser bias currents. The highest α parameters are found in the current range from 2.2 to 3.2 mA. For lower currents, the α parameters are up to a factor 4 smaller than the peak values in Fig. 6, which suggests a stronger intensity modulation. This is a contradiction to Fig. 1, which indicates a weak residual intensity modulation in the case $\omega_m > \omega_R$.

For the application within the CDSM magnetometer, a low first order asymmetry is desired. Therefore, two asymmetry thresholds are introduced which act as quality markers for the laser light spectrum. At $A_1 = \pm 0.5$ dB (Eq. 16) the first order side band amplitude ratio is above 0.89 and for $\pm$ 0.23 dB the side band amplitude ratio surpasses 0.95. An asymmetry below $\pm$ 0.23 dB is targeted for the instrument.

Figure 7 shows A_1 as a function of the laser bias current where the frequency modulation indices m_F are 1.50,

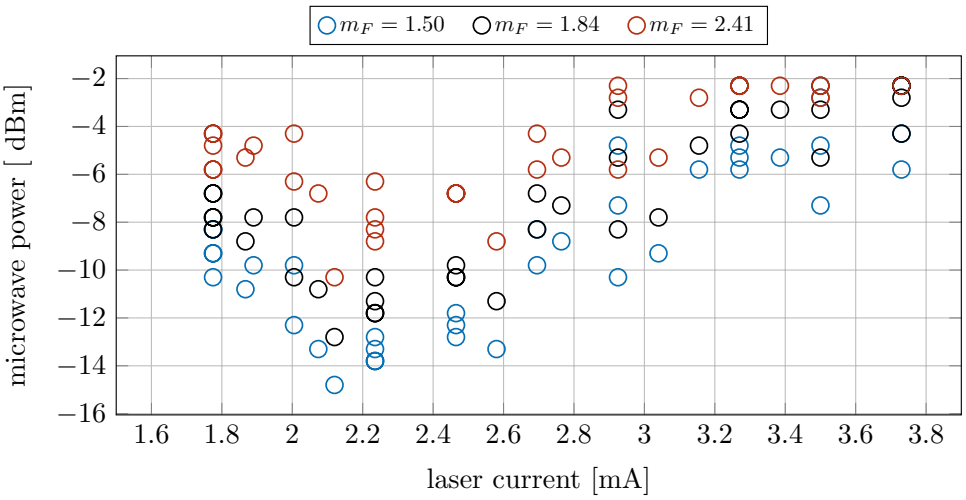

Fig. 5 The necessary modulation (microwave) power to achieve the FM indices $m_F = 1.50$, 1.84 and 2.41 as a function of laser current for all investigated VCSEL diodes. The highest modulation efficiency is found around 2.1 mA

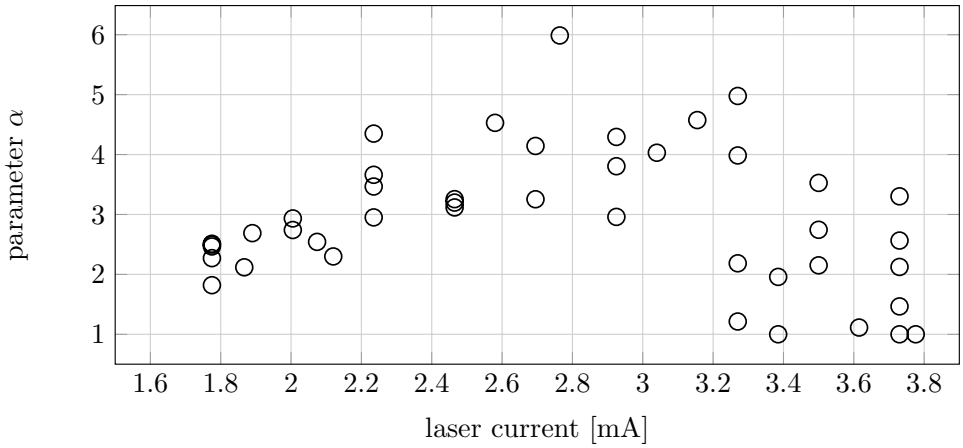

Fig. 6 The $\alpha = 2 \cdot m_F/m_I$ parameter as a function of laser current for the entire sample of laser diodes

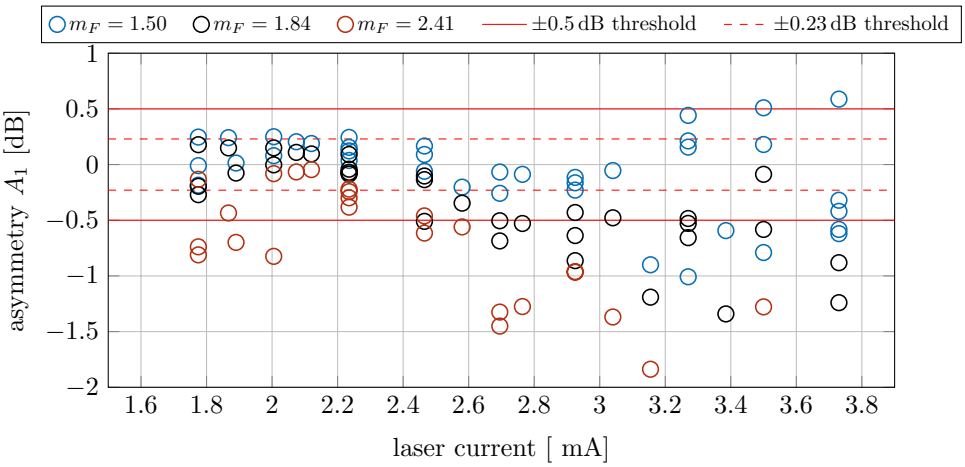

Fig. 7 First order side band asymmetry A_1 for the FM indices $m_F = 1.50$, 1.84 and 2.41 as a function of laser bias current. For an application a low first order amplitude asymmetry is of interest. The quality markers for the maximal allowed asymmetry at ± 0.5 dB and the ideal asymmetry below ± 0.23 dB are marked with horizontal lines

Table 1 Laser bias currents (with standard deviation) where the quality marker thresholds for the first order side band amplitude asymmetry A_1 are exceeded, listed for several FM indices m_F

m_F	−0.5 dB threshold [mA]	−0.23 dB threshold [mA]
1.50	/	2.7 ± 0.4
1.84	2.8 ± 0.3	2.4 ± 0.2
2.41	2.3 ± 0.3	2.3 ± 0.2

1.84 and 2.41. The horizontal lines are the quality marker thresholds. For the entire sample, the mean laser bias currents where the quality marker thresholds exceed the limits are listed in Table 1.

Starting at about 2.9 mA the asymmetry A_1 variations for $m_F = 1.50$ do not allow to calculate a mean laser bias current at which the −0.5 dB threshold is exceeded.

The CDSM utilises laser bias currents from about 1.6 to 3.8 mA. A standard deviation (see Table 1) in the range of 0.2 to 0.4 mA corresponds to a 10 to 20% variation in the maximum suitable laser bias current and therefore in the maximum usable optical output powers between the individual laser diodes. Some laser diodes never show an asymmetry below −0.5 dB at $m_F = 2.41$.

Figure 8 shows the maximal achievable frequency modulation index m_F^{max} which allows an asymmetry below the quality marker thresholds as a function of the laser bias current. For the additional threshold of −0.05 dB the ratio is larger than 0.98 and the first order side band amplitudes are considered to be equal.

Figure 8 is of practical interest, because it shows the usable operational parameter space of the entire laser diode sample under the restriction of the low first order asymmetry. For applications which require a FM index of $m_F = 2.41$ with a low first order asymmetry, only a very narrow laser bias current range around 2.1 mA is available for this sample of VCSEL diodes. The acceptance of higher asymmetries increases the suitable bias current range.

This limited laser bias current range defines the usable optical output power. If a low asymmetry is required for higher laser bias currents, a reduction of the FM index is necessary. However, a lower FM index will reduce the optical power within the first order side bands. Depending on

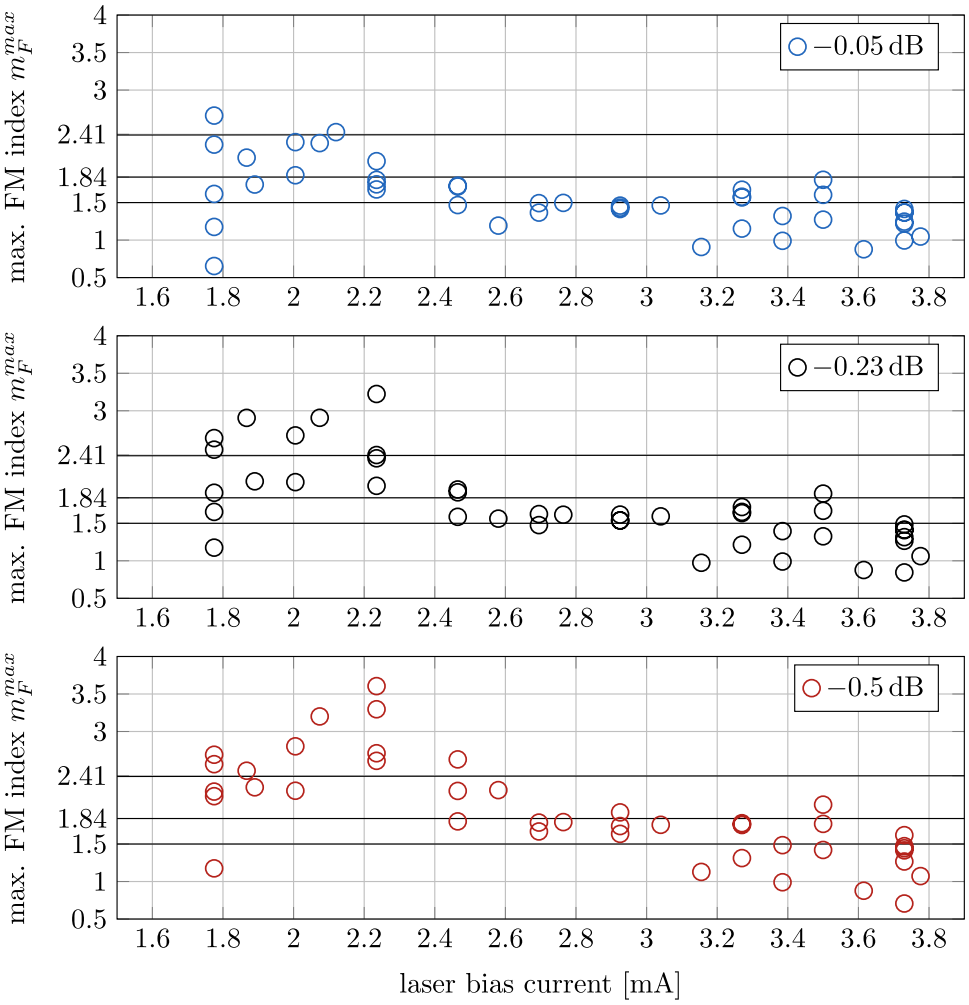

Fig. 8 The maximal suitable frequency modulation (FM) index m_F^{max} is displayed as a function of the applied laser bias current, which allows to operate the VCSEL diodes below the three asymmetry thresholds A_1: −0.05 dB, −0.23 dB and −0.5 dB. The entire sample of VCSEL diodes is considered

the individual VCSEL diode's modulation capability and its optical output power characteristics, an increase in laser bias current with a simultaneous reduction of the FM index could result in no or only a small increase of the desired optical power of the first order side bands, with the additional drawback of amplifying unwanted spectral components.

Despite the general modulation behaviours observed for the entire sample, the spread in the individual data points (Figs. 7 and 8) is found. Especially for large laser bias currents the modulation capability differences between the individual laser diodes becomes prominent. Therefore, a thorough spectral analysis of each VCSEL diode is necessary to guarantee the desired modulation behaviour.

7 Conclusion

This paper discusses the frequency and intensity modulation capabilities of a sample of 10 VCSEL diodes from one manufacturer. The modulations are introduced by direct laser current modulation and are analysed over a bias current range from 1.6 to 3.8 mA at the constant modulation frequency of 3.517 GHz.

The presented spectral evaluation and analysis focuses on the application of these diodes within an optically pumped magnetometer. The correct instrument operation requires first order side band amplitudes with a low asymmetry.

The theoretical evaluation is based on the dynamic small signal model which is in a good agreement with the measured modulation behaviour for lower laser bias currents where the relaxation resonance frequency ω_R is smaller than the modulation frequency ω_m. At high modulation currents (where $\omega_R > \omega_m$) and high modulation powers the modulation behaviour can not be fully explained by the dynamic small signal model.

Depending on the required first order side band amplitude symmetry and the required frequency modulation index, the suitable laser bias current range reduces to a small window. For the investigated sample, this window is at 2.1 ± 0.2 mA which is at about half of the maximum rating for the laser bias current of 4 mA. At this laser bias current range, the highest modulation efficiency is observed since $\omega_m \approx \omega_R$.

This range additionally limits the usable optical output power of the laser diodes.

The operation of the VCSEL diodes at other laser bias currents requires the reduction of the modulation indices to maintain the required symmetry of the first order side band amplitudes. At these laser bias currents the desired optical power within the first order side bands is reduced. This increases the carrier amplitude, which is not used for the application, resulting in the loss of effective optical power and in light shift effects caused by a non-resonant optical component with a strong amplitude.

The individual VCSEL diodes show a large and significant variation in their modulation capabilities, especially for large laser bias currents where the residual intensity modulation becomes prominent. Thus, from the perspective of an application within an instrument or within a laboratory experiment which require a well defined light source, the interchangeability of the individual laser diodes is not given. The analysis shows, that only a fraction of the sample's laser diodes is able to perform with the desired modulation capabilities. As a consequence, each individual VCSEL diode has to be preassessed and thoroughly tested in terms of its modulation capabilities to find the suitable operational parameters to achieve the required performance.

The found significant variations in the modulation capabilities suggest that VCSEL diodes with different packages, fabrication process or manufacturers are also subject to significant variations and a preassessment for each individual laser diode is necessary.

The selected VCSEL diode for the CDSM on board the JUICE mission features the lowest first order side band asymmetry for the largest possible laser bias current range at acceptable FM indices. This allows to utilise the high optical powers at high laser bias currents to combat additional damping within the optical fibres and the optical components which are accumulated during the years in space.

Acknowledgements Open access funding provided by Graz University of Technology.

Author Contributions All authors contributed to the study conception and design. Material preparation, data collection and analysis were performed by CA. The first draft of the manuscript was written by CA and all authors commented on previous versions of the manuscript. All authors read and approved the manuscript.

Funding Open access funding provided by Graz University of Technology. The authors are grateful for the financial support from the Austrian Space Applications Programme (Grant No. 882256) of the Austrian Research Promotion Agency and the PRODEX Programme of the European Space Agency (Grant No. 4000114669).

Code Availability The code generated during the current study is available from the corresponding author on reasonable request.

Materials Availability The datasets generated during and/or analysed during the current study are available from the corresponding author on reasonable request.

Declarations

Conflict of interest All authors certify that they have no affiliations with or involvement in any organization or entity with any financial interest or non-financial interest in the subject matter or materials discussed in this manuscript.

Consent to participate Not applicable.

Consent for publication Not applicable.

References

1. S. Kobayashi, Y. Yamamoto, M. Ito, T. Kimura, Direct frequency modulation in AIGaAs semiconductor lasers. IEEE Trans. Microw. Theory Tech. **30**(4), 428–441 (1982). https://doi.org/10.1109/TMTT.1982.1131084
2. R. Lammegger, Method and device for measuring magnetic fields. WO/2008/151344, (2008)
3. E. Arimondo, V Coherent Population Trapping in Laser Spectroscopy. Prog. Opt. **35**, 257–354 (1996). https://doi.org/10.1016/S0079-6638(08)70531-6
4. A. Pollinger, M. Ellmeier, W. Magnes, C. Hagen, W. Baumjohann, W. Leitgeb, R. Lammegger, Enable the inherent omni-directionality of an absolute coupled dark state magnetometer for e.g. scientific space applications. 2012 IEEE I2MTC - International Instrumentation and Measurement Technology Conference, Proceedings, 33–36 (2012). https://doi.org/10.1109/I2MTC.2012.6229247
5. A. Pollinger, R. Lammegger, W. Magnes, C. Hagen, M. Ellmeier, I. Jernej, M. Leichtfried, C. Kürbisch, R. Maierhofer, R. Wallner, G. Fremuth, C. Amtmann, A. Betzler, M. Delva, G. Prattes, W. Baumjohann, Coupled dark state magnetometer for the China Seismo-Electromagnetic Satellite. Measure. Sci. Technol. (2018). https://doi.org/10.1088/1361-6501/aacde4
6. T.L. Paoli, J.E. Ripper, Direct modulation of semiconductor lasers. Proc. IEEE **58**(10), 1457–1465 (1970). https://doi.org/10.1109/PROC.1970.7971
7. C.M. Long, K.D. Choquette, Optical characterization of a vertical cavity surface emitting laser for a coherent population trapping frequency reference. J. Appl. Phys. (2008). https://doi.org/10.1063/1.2838175
8. A. Pollinger, C. Amtmann, A. Betzler, B. Cheng, M. Ellmeier, C. Hagen, I. Jernej, R. Lammegger, B. Zhou, W. Magnes, In-orbit results of the Coupled Dark State Magnetometer aboard the China Seismo-Electromagnetic Satellite. Geosci. Instrument.

Methods Data Syst. **9**(2), 275–291 (2020). https://doi.org/10.5194/gi-9-275-2020
9. O. Grasset, M.K. Dougherty, A. Coustenis, E.J. Bunce, C. Erd, D. Titov, M. Blanc, A. Coates, P. Drossart, L.N. Fletcher, H. Hussmann, R. Jaumann, N. Krupp, J.P. Lebreton, O. Prieto-Ballesteros, P. Tortora, F. Tosi, T. Van Hoolst, JUpiter ICy moons Explorer (JUICE): An ESA mission to orbit Ganymede and to characterise the Jupiter system. Planet. Space Sci. **78**, 1–21 (2013). https://doi.org/10.1016/j.pss.2012.12.002
10. M. Ellmeier, C. Hagen, J. Piris, R. Lammegger, I. Jernej, M. Woschank, W. Magnes, E. Murphy, A. Pollinger, C. Erd, W. Baumjohann, L. Windholz, Accelerated endurance test of single-mode vertical-cavity surface-emitting lasers under vacuum used for a scalar space magnetometer. Appl. Phys. B: Lasers Optics (2018). https://doi.org/10.1007/s00340-017-6889-2
11. F. Levi, A. Godone, J. Vanier, The light shift effect in the coherent population trapping cesium maser. IEEE Trans. Ultrason. Ferroelectr. Freq. Control **47**(2), 466 (2000). https://doi.org/10.1109/58.827437
12. A.O. Makarov, S.M. Ignatovich, V.I. Vishnyakov, I.S. Mesenzova, D.V. Brazhnikov, N.L. Kvashnin, M.N. Skvortsov, Investigation of commercial 894.6 nm vertical-cavity surface-emitting lasers for applications in quantum metrology. AIP Conf. Proc. (2019). https://doi.org/10.1063/1.5098154
13. J. Vanier, A. Godone, F. Levi, Coherent microwave emission in coherent population trapping: origin of the energy and of the quadratic light shift. In: Proceedings of the 1999 Joint Meeting of the European Frequency and Time Forum and the IEEE International Frequency Control Symposium (Cat. No.99CH36313), vol. 1, pp. 96–991 (1999). https://doi.org/10.1109/FREQ.1999.840716
14. F. Levi, A. Godone, J. Vanier, S. Micalizio, G. Modugno, Lineshape of dark line and maser emission profile in CPT. Eur. Phys. J. D **12**(1), 53–59 (2000). https://doi.org/10.1007/s100530070042
15. L.A. Coldren, S.W. Corzine, M.L. Mashanovitch, *Diode Lasers and Photonic Integrated Circuits* (John Wiley & Sons, Hoboken, 2012). https://doi.org/10.1002/9781118148167
16. H. Olesen, G.A. Jacobsen, A theoretical and experimental analysis of modulated laser fields and power spectra. IEEE J. Quantum Electron. **18**(12), 2069–2080 (1982). https://doi.org/10.1109/JQE.1982.1071490
17. A. Al-samaneh, VCSELs for cesium-based miniaturized atomic clocks. PhD thesis, Universität Ulm und Technischen Hochschule (2014). https://doi.org/10.18725/OPARU-3205
18. I. Jernej, M. Faust, R. Lammegger, I.A. McKenzie, J. Kuhnhenn, C. Knothe, S. O'Riorden, J. Barbero, P. Brown, V. Lelievre, M. Agú, A. Alessi, C. Amtmann, A. Betzler, M. Dougherty, M. Ellmeier, C. Hagen, A. Hauser, M. Hartig, A. Lamott, M. Leichtfried, W. Magnes, A. Mahapatra, S. Mariojouls, D. Monteiro, A. Pollinger, A., Salomon, U. Weinand, R. Wolf, Design and test of the optical fiber assemblies for the scalar magnetic field sensor aboard the JUICE mission. In: Proc. SPIE 11852, International Conference on Space Optics - ICSO 2020, 1185264 (2021). https://doi.org/10.1117/12.2600052
19. U. Tietze, C. Schenk, E. Gamm, *Halbleiter-Schaltungstechnik*, 16th edn. (Springer, Berlin, 2019)
20. F. Gruet, A. Al-Samaneh, E. Kroemer, L. Bimboes, D. Miletic, C. Affolderbach, D. Wahl, R. Boudot, G. Mileti, R. Michalzik, Metrological characterization of custom-designed 894.6 nm vcsels for miniature atomic clocks. Opt. Express **21**(5), 5781–5792 (2013). https://doi.org/10.1364/OE.21.005781